Theoretical study of the hydroxylation of phenolates by the Cu2O2(N,N′-dimethylethylenediamine)2 2+ complex

ARTICLE *in* EUROPEAN JOURNAL OF BIOCHEMISTRY · NOVEMBER 2008

Impact Factor: 2.54 · DOI: 10.1007/s00775-008-0443-y · Source: PubMed

4 AUTHORS, INCLUDING:

Josep M. Luis
Universitat de Girona
106 PUBLICATIONS **2,456** CITATIONS
SEE PROFILE

Miquel Solà
Universitat de Girona
398 PUBLICATIONS **8,667** CITATIONS
SEE PROFILE

J Biol Inorg Chem (2009) 14:229–242
DOI 10.1007/s00775-008-0443-y

ORIGINAL PAPER

Theoretical study of the hydroxylation of phenolates by the Cu_2O_2(*N*,*N*′-dimethylethylenediamine)$_2^{2+}$ complex

Mireia Güell · Josep M. Luis · Miquel Solà · Per E. M. Siegbahn

Received: 30 May 2008 / Accepted: 8 October 2008 / Published online: 30 October 2008

Abstract Tyrosinase catalyzes the *ortho* hydroxylation of monophenols and the subsequent oxidation of the diphenolic products to the resulting quinones. In efforts to create biomimetic copper complexes that can oxidize C–H bonds, Stack and coworkers recently reported a synthetic μ-η^2:η^2-peroxodicopper(II)(DBED)$_2$ complex (DBED is *N*,*N*′-di-*tert*-butylethylenediamine), which rapidly hydroxylates phenolates. A reactive intermediate consistent with a bis-μ-oxo-dicopper(III)-phenolate complex, with the O–O bond fully cleaved, is observed experimentally. Overall, the evidence for sequential O–O bond cleavage and C–O bond formation in this synthetic complex suggests an alternative mechanism to the concerted or late-stage O–O bond scission generally accepted for the phenol hydroxylation reaction performed by tyrosinase. In this work, the reaction mechanism of this peroxodicopper(II) complex was studied with hybrid density functional methods by replacing DBED in the μ-η^2:η^2-peroxodicopper(II)(DBED)$_2$ complex by *N*,*N*′-dimethylethylenediamine ligands to reduce the computational costs. The reaction mechanism obtained is compared with the existing proposals for the catalytic *ortho* hydroxylation of monophenol and the subsequent oxidation of the diphenolic product to the resulting quinone with the aim of gaining some understanding about the copper-promoted oxidation processes mediated by 2:1 Cu(I)O_2-derived species.

Keywords Tyrosinase · Copper enzymes · Biomimetic metal complexes · O_2 cleavage · Density functional theory

Electronic supplementary material The online version of this article (doi:10.1007/s00775-008-0443-y) contains supplementary material, which is available to authorized users.

M. Güell · J. M. Luis · M. Solà (✉)
Departament de Química,
Institut de Química Computacional,
Universitat de Girona,
Campus de Montilivi,
17071 Girona, Spain
e-mail: miquel.sola@udg.edu

M. Güell · P. E. M. Siegbahn (✉)
Department of Biochemistry and Biophysics,
Stockholm University,
106 91 Stockholm, Sweden
e-mail: ps@physto.se

Introduction

Proteins containing copper ions at their active site are usually involved as redox catalysts in a wide range of biological processes. Type-3 active site copper-containing proteins have a dicopper core, in which both copper ions are surrounded by three nitrogen donor atoms from histidine residues [1, 2]. They are able to reversibly bind dioxygen at ambient conditions. The copper(II) ions in the oxy state of these proteins are strongly antiferromagnetically coupled, leading to an EPR-silent behavior. This class of enzymes is represented by three proteins, namely, hemocyanin, catechol oxidase, and tyrosinase.

Tyrosinase is found in vegetables, fruits, and mushrooms, where it is a key enzyme in the browning that occurs upon bruising or long-term storage. In mammals, the enzyme is responsible for skin pigmentation abnormalities, such as flecks and defects [3]. Recently, the enzyme was reported to be linked to Parkinson disease and other neurodegenerative diseases [4, 5]. Thus, tyrosinase is quite significant in the fields of medicine, agriculture, and industry [6, 7].

Tyrosinase catalyzes the *ortho* hydroxylation of monophenols and the subsequent oxidation of the diphenolic

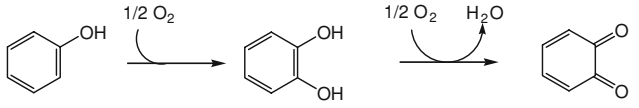

Scheme 1 Mechanism of the oxygenation and oxidation catalyzed by tyrosinase

products to the resulting quinones (Scheme 1). Little is known about the mechanistic details of the monooxygenase (phenolase) activity of tyrosinase. The enzymatic reaction is very complicated, involving many fundamental catalytic processes, and it is blinded by significant side reactions such as nonenzymatic transformations of *o*-quinone products to melanin pigments [8]. At least three different mechanisms for the oxidation of phenols to *o*-quinones have been suggested.

First, in the mechanism proposed by Solomon and coworkers [9] in 1985, the monophenol binds to the axial position of one of the coppers of the oxy site (Scheme 2). Then it undergoes a trigonal bipyramidal rearrangement towards the equatorial plane, which orients its *ortho* position for hydroxylation by the peroxide. This generates a coordinated *o*-diphenolate, which is oxidized to the quinone, resulting in a deoxy site ready for further dioxygen binding.

Second, another mechanism for the oxidation of phenols to *o*-quinones catalyzed by tyrosinase was suggested from calculations using the hybrid density functional theory (DFT) B3LYP method [10]. In the proposed mechanism (Scheme 3), the bridging hydroxide abstracts a proton from the tyrosine substrate. Then dioxygen replaces the bridging water. Subsequently, the dioxygen attacks the phenolate ring, which is followed by the O–O bond cleavage. In the end, the bridging oxygen abstracts a proton from the substrate, the quinone is formed, and the catalytic cycle can start again.

Finally, on the basis of the crystal structure of tyrosinase [11], another mechanism was suggested (Scheme 4). In this mechanism, a peroxide ion, which forms a bridge with two Cu(II) ions in the oxy form of tyrosinase, acts as a catalytic base. As a result, a proton is abstracted by the peroxide

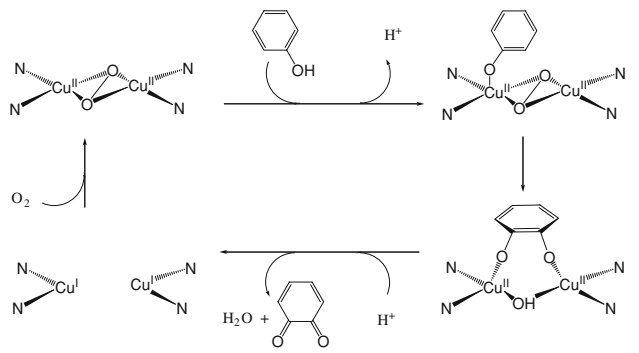

Scheme 2 Catalytic cycle for the monooxygenation of monophenols to *o*-quinones by tyrosinase suggested by Solomon and coworkers [9]

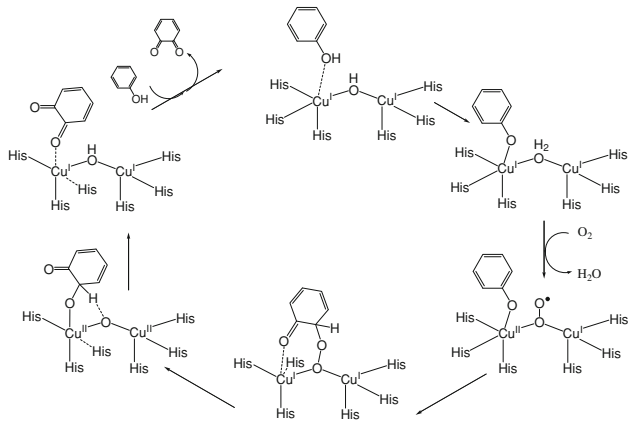

Scheme 3 Catalytic cycle of tyrosinase suggested on the basis of hybrid density functional theory calculations [10]

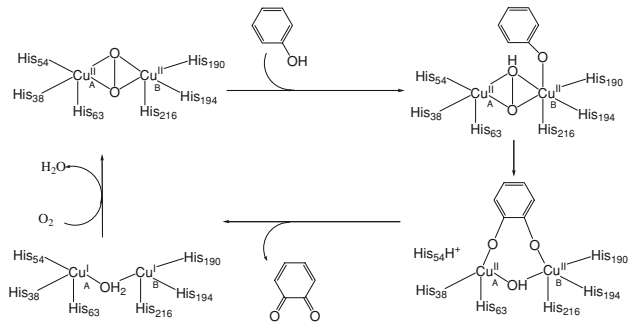

Scheme 4 Structure-based catalytic mechanism of tyrosinase suggested by Matoba et al. [11]

from the phenolic hydroxyl. Subsequently, the deprotonated oxygen atom of monophenol binds to Cu_B at the sixth coordination site. At this stage, Cu_B is hexacoordinated in a tetragonal bipyramidal cage. One of the two peroxide oxygens is then added to the *ortho* carbon of monophenol. This monooxygenase reaction should be accelerated by the formation of a stable intermediate, in which the newly generated oxygen atom of diphenol binds to Cu_A. To form this state, His54, which is an axial ligand to Cu_A, must be released from the current position. This assumption is derived from the flexible feature of the His54 residue in the copper-free and copper(II)-bound oxy forms. Simultaneously, His54 can act as a catalytic base for the deprotonation from the substrate. The resulting intermediate should easily be able to transfer two electrons to copper, resulting in the formation of the deoxy form of tyrosinase and quinone.

The order in which the O–O bond cleavage and the attack on the ring take place is not specified in the first and the third proposals described for the mechanism of tyrosinase. It is well known that the side-on μ-η^2:η^2-peroxo species that appears in these mechanisms has an unusual electronic structure which activates it for the hydroxylation

reaction [1]. The peroxide moiety is more electrophilic than in the end-on peroxycopper(II) complex because of its strong σ donation to the copper ions [12–14]. Moreover, the peroxide σ^* orbital participates in the back-donation from the copper ions and consequently it weakens the O–O bond [12–14]. Besides, coordination of the monophenolic substrate would donate additional electron density into this electrophilic center and foster the hydroxylation reaction. In oxytyrosinase, the O–O bond in the oxygen intermediate involved in the best characterized metalloenzyme hydroxylation reactions is still present [15]. Nevertheless, the direct coordination of the substrate to the copper in tyrosinase can perturb the peroxodicopper core bonding by donating electron density, which should facilitate O–O bond breaking, and also by transferring its acidic proton to the peroxide. In general, it remains an open question whether the O–O bond is cleaved prior to, concerted with, or after the attack on the ring that leads to the formation of a new C–O bond (Scheme 5).

The high efficiency of tyrosinase in the usually difficult C–H oxidation has elicited extensive synthetic efforts to create copper complexes that can oxidize C–H bonds [16–25]. Karlin et al. [26–29] studied copper binuclear complexes that showed C–H aromatic bond activation chemistry, similar to monooxygenase action. Using phenolates as substrates, a number of other research groups have described a variety of interesting and important monophenolase activity model studies [16, 30, 31]. These studies have either involved μ-η^2:η^2-peroxodicopper(II) or bis-μ-oxodicopper(III) complex reactions, leading to catechol or quinone products. Since it has been shown that the interconversion is rapid [16, 32, 33], it is difficult to know which isomeric form is the active species in *o*-phenol hydroxylation.

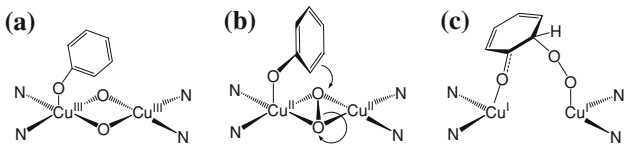

Scheme 5 Three possible mechanistic scenarios for the monooxygenation of phenol by oxytyrosinase. **a** The O–O bond cleaves prior to the attack on the ring, yielding a species which is the formally binuclear copper(III) bis-μ-oxo complex; **b** O–O bond cleavage is concerted with the attack on the ring; **c** the O–O bond is still present after attack on the ring, yielding an aryl peroxide intermediate [1]

Recently, Stack and coworkers [31] reported a synthetic μ-η^2:η^2-peroxodicopper(II) complex, with an absorption spectrum similar to that of the enzymatic active oxidant, which rapidly hydroxylates phenolates at −80 °C. Upon phenolate addition at extremely low temperature in solution (−120 °C), a reactive intermediate **A** consistent with a bis-μ-oxodicopper(III)-phenolate complex, with the O–O bond fully cleaved, was observed experimentally (Scheme 6). The subsequent hydroxylation step had the hallmarks of an electrophilic aromatic substitution mechanism, similar to that for tyrosinase. Overall, the evidence for sequential O–O bond cleavage and C–O bond formation in this synthetic complex suggests an alternative mechanism to the concerted or late-stage O–O bond scission generally accepted for the phenol hydroxylation reaction performed by tyrosinase.

In this work, hybrid DFT calculations were carried out to investigate the reaction mechanism for a model of the peroxodicopper(II) complex synthesized by Stack and coworkers [31], in which the *tert*-butyl groups were replaced by methyl groups to reduce the computational cost. This model was chosen to be as energetically representative as possible of the system studied (vide infra). The mechanism proposed in this work is compared with the existing proposals for the catalytic mechanism of the enzyme with the aim of gaining a deeper understanding about the chemical and biological copper-promoted oxidation processes with 2:1 $Cu(I)O_2$-derived species.

Methods

All the calculations were done using the B3LYP [34, 35] hybrid density functional. Open-shell systems were treated using broken-symmetry unrestricted DFT. For the open-shell structures, both the open-shell singlet and the triplet states were considered. Geometry optimizations were performed using a standard-valence LACVP basis set as implemented in the Jaguar 5.5 program [36]. For the first- and second-row elements, LACVP implies a 6-31G double-ξ basis set. For the copper atoms, LACVP uses a nonrelativistic effective core potential [37] and the valence part is described by a double-ξ basis set. Local minima were optimized using the Jaguar 5.5 program [36]. Transition states and analytical Hessians for all the stationary

Scheme 6 Experimental results obtained by Stack and coworkers [31]

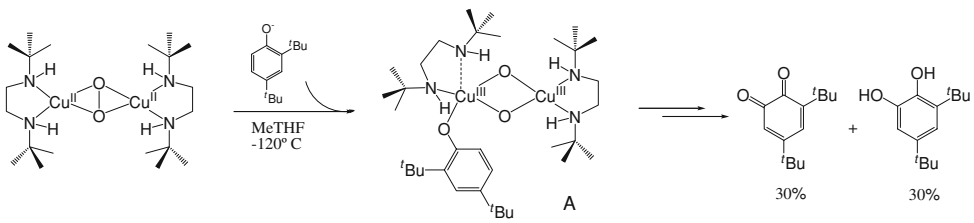

points (second derivatives of the energy with respect to the nuclear coordinates) were obtained using the Gaussian 03 program [38] with the same functional and basis set. The Hessians were used to determine the nature of each stationary point and to calculate zero-point energies, thermal corrections, and entropy effects. These last two terms were computed at −120 °C. Accurate single-point energies were obtained using the cc-pVTZ(−f) basis set [39, 40]. For the copper atoms the lacv3p+ effective core potential was used. The self-consistent reaction field method implemented in Jaguar 5.5 was used to evaluate electrostatic solvation effects and compute solvent free energies [41, 42]. For the solvent methyltetrahydrofuran, a dielectric constant of 7.0 was used and the probe radius was set to 2.71 Å and the lacvp* basis set was used. Final free energies given in this work include energies computed at the B3LYP/cc-pVTZ(−f)&lacv3p+//B3LYP/lacvp level of theory together with solvent effects obtained with the B3LYP/lacvp* method and with zero-point energies and thermal and entropy corrections calculated with the B3LYP/lacvp method at −120 °C.

In the literature there are several benchmark tests on the accuracy of the B3LYP functional [43]. On the basis of these results, an average error of 3–5 kcal/mol is expected for the computed relative energies for transition-metal-containing systems [44]. There are indications that the reparameterized B3LYP* functional, which uses 15% of exact Hartree–Fock (HF) exchange as compared to the 20% used in the original functional, gives a better description of the relative energies in transition-metal-containing systems [45, 46]. Therefore, the B3LYP* functional was used to check all of the relative energies discussed below.

To study in detail the mechanism of the hydroxylation of an aromatic ring mediated by the peroxodicopper complex reported by Stack and coworkers [31], we created a simplified model of the system. In particular, the *tert*-butyl substituents of the experimental complex were replaced by methyl groups. Consequently, the model has *N*,*N*′-dimethylethylenediamine (DMED) ligands instead of *N*,*N*′-di-*tert*-butylethylenediamine (DBED). Furthermore, the phenolate, instead of the 2,4-di-*tert*-butylphenolate used experimentally, was used as the substrate of the reaction. Introducing these modifications, we are changing the system and we are aware that they could have some effect on the mechanism. The experimental complex and the system used in the present calculations are shown in Fig. 1. In the new model, the geometry of the core and the spin density values are almost identical to the ones of the complete system (Table 1). Moreover, experimentally it has been found that the peroxo form of DBED has a Cu–Cu distance of 3.45 Å [31], which agrees with the results obtained here. In both cases Mulliken atomic spins of +0.43 and −0.43 on the copper atoms in the most stable open-shell singlet species are consistent with antiferromagnetic coupling of the two Cu(II) ions.

When systems with a $Cu_2O_2^{2+}$ core are studied, it is important to determine correctly the most stable coordination mode of O_2 binding to the two copper atoms [47–53]. This is usually a difficult task for DFT methods [54]. Experimentally, it was reported that the $Cu_2O_2(DBED)_2^{2+}$ complex consists of 95% side-on peroxo and 5% bis-μ-oxo before the interaction with the phenolate [31, 55, 56]. When the B3LYP method is used with the present model, the energy difference between the peroxo and the bis-μ-oxo forms is only 2.5 kcal/mol, the bis-μ-oxo form being slightly more stable. Although the B3LYP study of our model complex does not give the μ-η^2:η^2-peroxodicopper(II) form as the most stable complex, the small energy difference found between the two species indicates that the two species are almost isoenergetic, in line with experimental results.

To explore the effect of increasing the degree of HF exchange in hybrid methods, we calculated the optimized geometries of the peroxo and bis-μ-oxo structures for the system by varying monotonically the proportion of exact exchange introduced in B3LYP-like functionals.

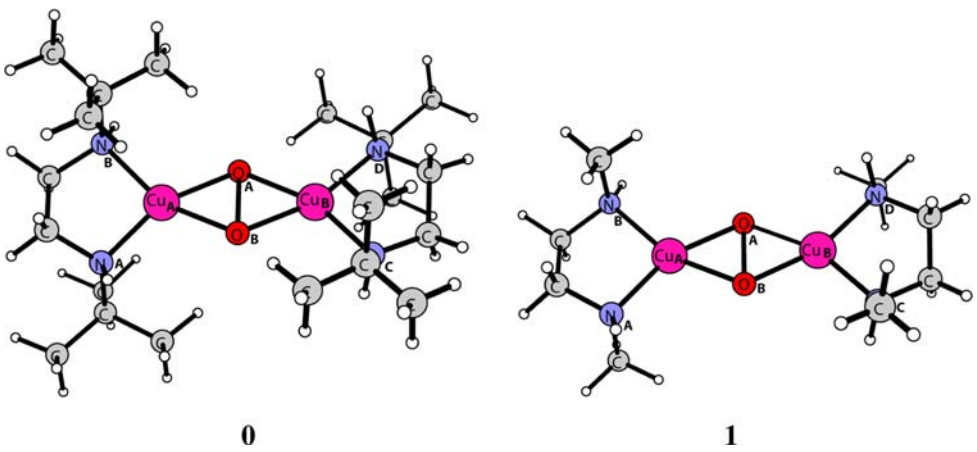

Fig. 1 Synthetic μ-η^2:η^2-peroxodicopper(II) complex studied by Stack and coworkers [31] (*left*) and the model of the system used in this study (*right*)

Table 1 Comparison of geometrical parameters and spin density populations for the synthetic μ-η^2:η^2-peroxodicopper(II) complex studied by Stack and coworkers [31] (**0**) and the model of this system used in the present study (**1**)

Structures	Multiplicity	Distances (Å)						Spin density			
		Cu_A–O_A	Cu_A–O_B	Cu_B–O_A	Cu_B–O_B	Cu_A–Cu_B	O_A–O_B	Cu_A	Cu_B	O_A	O_B
0	so	1.99	1.99	1.99	1.99	3.66	1.57	0.43	−0.43	0.00	0.00
	t	2.03	2.03	2.03	2.03	3.53	1.54	0.43	0.43	0.35	0.35
1	so	1.97	1.97	1.97	1.97	3.61	1.58	0.43	−0.43	0.00	0.00
	t	2.02	2.02	2.02	2.02	3.52	1.55	0.43	0.43	0.36	0.36

The structures are shown in Fig. 1

so open-shell singlet state, *t* triplet state

The nonlocal hybrid Becke's three parameter exchange functional (B3) [34] used in B3LYP was originally formulated as

$$E_{XC} = E_X^{LSDA} + a_o\left(E_X^{exact} - E_X^{LSDA}\right) + a_x\Delta E_X^{B88} + a_c\Delta E_C^{PW91}. \quad (1)$$

The E_X^{exact}, E_X^{LSDA}, ΔE_X^{B88}, and ΔE_C^{PW91} terms are the HF exchange energy based on Kohn–Sham orbitals, the uniform electron gas exchange–correlation energy, Becke's 1988 gradient correction for exchange [57], and the 1991 Perdew and Wang gradient correction to correlation [58, 59], respectively. The coefficients a_o, a_x, and a_c were determined by Becke [34] by a linear least-squares fit to 56 experimental atomization energies, 42 ionization potentials, and eight proton affinities. The values thus obtained were $a_o = 0.20$, $a_x = 0.72$, and $a_c = 0.81$. In the Gaussian 03 [38] implementation, the expression of the B3LYP functional is similar to Eq. 2, with some minor differences [60]:

$$E_{XC} = E_X^{LSDA} + a_o\left(E_X^{exact} - E_X^{LSDA}\right) + a_x\Delta E_X^{B88} + E_C^{VWN} + a_c\left(\Delta E_C^{LYP} - E_C^{VWN}\right). \quad (2)$$

In this equation, the Perdew and Wang correlation functional originally used by Becke is replaced by the Lee–Yang–Parr (LYP) [35] one. Since the LYP functional already contains a local part and a gradient correction, one has to remove the local part to obtain a coherent implementation. This can be done in an approximate way by subtracting E_C^{VWN} from ΔE_C^{LYP}. Note that in the Gaussian 03 implementation the VWN functional is the one derived by Vosko et al. [61, 62] from a fit to the random phase approximation results.

Results and discussion

Some authors claim that comparisons of bis-μ-oxo with side-on peroxo energies should be made with pure functionals containing no HF exchange [48, 63]. To study the dependence of the energy difference between the μ-η^2:η^2-peroxodicooper(II) and the bis-μ-oxo forms on the degree of HF exchange of the functional, we used the Gaussian 03 program feature that allows one to vary the B3LYP standard Becke parameter set through internal options. We changed the a_o parameter in 0.100 increments in the interval $0.000 \leq a_o \leq 0.5$, with fixed $a_x = 1 - a_o$ and $a_c = a_x$. The $a_x = 1 - a_o$ relationship has already been used in some hybrid functionals [64, 65]. In Table 2, we show the different parameter sets $\{a_o, a_x, a_c\}$ employed and the difference in free energy between the peroxo and the bis-μ-oxo isomers.

From the free energies of optimized isomers with the different parameter sets shown in Table 2, we can see that, in our $Cu_2O_2(DMED)_2^{2+}$ complex, when the pure functional BLYP is used (parameter set 0, in Table 2), the bis-μ-oxo isomer is 17.6 kcal/mol more stable than the peroxo isomer. The more the degree of HF exchange, the more stable the peroxo form of the studied complex is. This is in line with the previous results of Gherman and Cramer [54]. It should be remarked that parameter set 2, whose parameters are the most similar to those used in B3LYP, is the one that best reproduces the experimental results for the $Cu_2O_2(DBED)_2^{2+}$ species, showing that the energy difference between the two isomers is small. In a previous study [55], it was shown that geometry optimizations of the

Table 2 Parameter sets employed for B3LYP calculations and the corresponding relative free energies (kcal/mol) of the peroxo form as compared with the bis-μ-oxo isomer in the $Cu_2O_2(DMED)_2^{2+}$ complex (DMED is *N*,*N*′-dimethylethylenediamine)

Parameter set	a_0	a_x	a_c	ΔG
0[a]	0.000	1.000	1.000	17.6
1	0.100	0.900	0.900	9.1
2	0.200	0.800	0.800	−0.2
3	0.300	0.700	0.700	−12.0
4	0.400	0.600	0.600	−23.6
5	0.500	0.500	0.500	−26.8

[a] This parameter set corresponds to the BLYP functional

Table 3 Spin density at different spin states for the structures that intervene in the core isomerization of Cu_2O_2 for model of the complex before (**1**, TS12, **2**) and after (**2′**, TS2′3, **3**) the addition of the substrate

Structures	Multiplicity	Spin density					ΔG
		Cu_A	Cu_B	O_A	O_B	Substrate	
1 + PhO^-	so	0.43	−0.43	0.00	0.00	–	0.0
	t	0.43	0.43	0.36	0.36	–	1.9
TS12 + PhO^{-a}	so	0.28	−0.28	0.00	0.00	–	9.6
2 + PhO^{-a}	s	–	–	–	–	–	−2.5
2′	so	0.50	−0.39	−0.07	−0.27	0.04	−31.4
	t	0.38	0.49	0.36	0.31	0.04	−31.2
TS2′3[a]	so	0.40	−0.37	−0.08	−0.05	−0.11	−9.2
3[a]	s	–	–	–	–	–	−18.8

Calculated free energies (G), relative to structure **1** plus phenolate, in kilocalories per mole are also reported

so open-shell singlet state, *s* closed-shell singlet state, *t* triplet state

[a] Only the singlet is reported, since the triplet for these structures lies much higher in energy

peroxo species computed with the HF method and pure DFT methods either gave unreasonable geometrical parameters or converged to the bis-μ-oxo isomer. On the other hand, hybrid DFT methods reproduced nicely the measured geometrical parameters. Consequently, we consider that B3LYP is a suitable method to carry out the study of the mechanism with our model.

The present study of the reaction mechanism of our model for the $Cu_2O_2(DBED)_2^{2+}$ complex starts from the open-shell singlet peroxo form, which is the predominant one found experimentally [31]. From this point on, two different pathways are possible. In the first one (**1** → **2** → **3**), the O–O bond cleavage is prior to the binding of the substrate with the complex. In the second one (**1** → **2′** → **3**), the O–O bond cleavage takes place after the interaction of the substrate with the complex (Scheme 7).

Our results for the **1** → **2** → **3** pathway showed that the barrier for the O–O bond cleavage before the phenolate is bound (TS12) is 9.6 kcal/mol. The low energy barrier of 9.6 kcal/mol found for the interconversion between the peroxo and bis-μ-oxo forms in our model systems indicates that, at this temperature, the two isomers are in equilibrium, and, therefore, the transformation of the peroxo to the bis-μ-oxo form is possible (a half-lifetime of 11.2 s is obtained for the **1** → **2** conversion in our $Cu_2O_2(DMED)_2^{2+}$ peroxo model form using the expressions derived from transition state theory [66]). At this point, it should be mentioned that the theoretical barrier for the interconversion between the peroxo and bis-μ-oxo forms in the whole complex, i.e., $Cu_2O_2(DBED)_2^{2+}$, was found to be around 10 kcal/mol, which agrees with the value obtained for our model [55]. It is worth noting here that the calculations of Stack and coworkers have some limitations since they were carried out only for the lowest spin state energy, without including the solvent effects, and with a partial optimization of the transition state (instead the authors took the point of maximum energy along a linear transit that transforms **1** into **2**). The next stage of the reaction is the

Scheme 7 Two possible ways in which O–O can be cleaved in the system studied, before and after the binding with the substrate

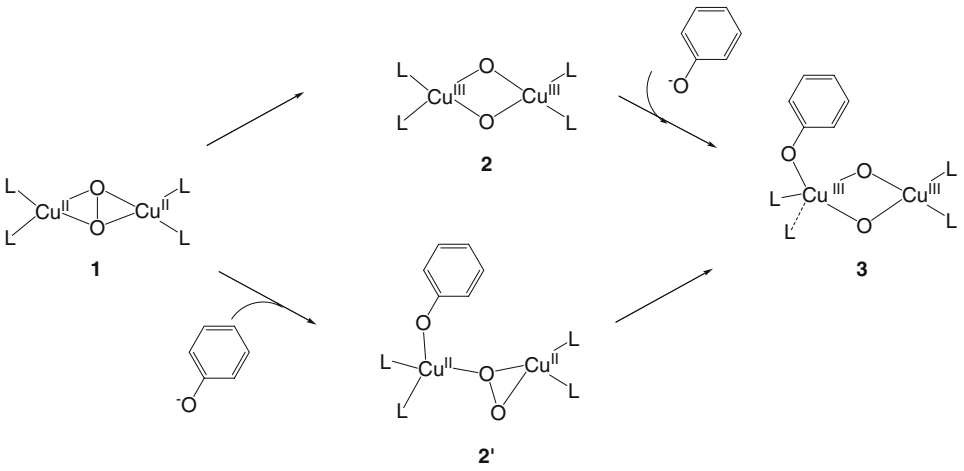

binding of the phenolate with the complex that would lead from structure **2** to structure **3**. This step was found to be exothermic by around 16 kcal/mol (Table 3). It should be emphasized that, for the $Cu_2O_2(DBED)_2^{2+}$ complex, the experimental energy difference between the peroxo and bis-μ-oxo isomers with sterically demanding neutral ligands is small [16, 32, 67–69], slightly favoring the peroxo form. In fact, in their work at −120 °C, Stack and coworkers [31] detected that 95% of the dicopper(II) complex was present as the peroxo isomer (species **0** in Fig. 1) and 5% as the bis-μ-oxo form [55, 56].

For the second possible pathway (**1** → **2′** → **3**), the free energy of binding of the substrate to the peroxo form (structure **1**) of the complex is exothermic by 31.4 kcal/mol. The next step would be the O–O bond cleavage with the substrate bound to the biomimetic complex (TS2′3), which has a barrier of more than 20 kcal/mol. This barrier is quite high since two bonds are simultaneously weakened. The O–O bond cleaves assisted basically by a single copper atom and, at the same time, the distance between the copper with the substrate bound and one of the nitrogen atoms of the ligand (Cu_A–N_B) increases considerably (Table 4, Fig. 2).

As said before, the low energy barrier for the interconversion between the μ-η^2:η^2-peroxodicopper(II) and the bis-μ-oxodicopper(II) isomers suggests that these two forms are in equilibrium at −120 °C. Although our theoretical calculated energies favor slightly the bis-μ-oxo form, the experimental results for species **0** in Fig. 1 indicate that this equilibrium is displaced towards the peroxo isomer [31, 55, 56]. The added phenolate can react with any of the two forms since reactions of phenolate with the peroxo and bis-μ-oxo isomers are exothermic processes with reaction free energies of −30.8 and −16.3 kcal/mol, respectively. In the absence of any other kinetic constraint, the added phenolate will react with the peroxo form according to the experimental observation of this species in solution [31] or with the bis-μ-oxo isomer as indicated by our calculations. It is worth mentioning that, for the addition of fragments of different charge (such as addition of phenolate to species **1** or **2**), solvent effects are extremely important and difficult to handle correctly. For this reason, we consider that to definitely differentiate between routes **1** → **2** → **3** and **1** → **2′** → **3** further calculations including explicitly solvent molecules in the model are necessary. In addition, a study of the reaction dynamics might be necessary to reach a final answer about this initial part of the reaction mechanism. At the present stage, solvent effects were introduced using an approximate polarizable continuum model. The approximate nature of such calculations prevents us from definitely rejecting either of the two pathways proposed.

Experimentally, an intermediate where the distance between the two copper ions is 2.79 Å and with an average distance of 1.89 Å between each copper and the four nitrogen/oxygen ligands was detected (species **A** in Scheme 6) [31]. The observed structure should correspond to structure **3**, which has a distance of 2.86 Å between the

Table 4 Comparison of geometrical parameters for the transition states of the O–O bond cleavage, TS12 and TS2′3

Structures	Distances (Å)									
	Cu_A–O_A	Cu_A–O_B	Cu_B–O_A	Cu_B–O_B	Cu_A–Cu_B	O_A–O_B	Cu_A–N_A	Cu_A–N_B	Cu_B–N_C	C_B–N_D
TS12	1.87	1.87	1.87	1.87	3.16	2.01	2.00	2.00	2.00	2.00
TS2′3	1.91	1.98	1.89	1.90	3.34	1.88	2.06	2.30	2.06	2.06

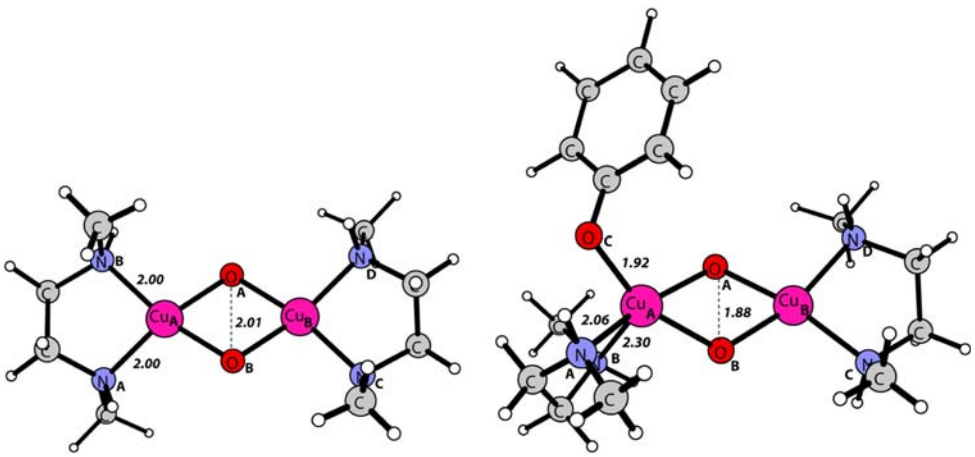

Fig. 2 Fully optimized transition states for the O–O bond cleavage TS12 and TS2′3. Distances are in angstroms

Table 5 Comparison of geometrical parameters of the transition state for the structures that intervene in the C–O bond formation

Structures	Multiplicity	Distances (Å)											
		Cu_A–O_A	Cu_A–O_B	Cu_B–O_A	Cu_B–O_B	Cu_A–Cu_B	O_A–O_B	Cu_A–O_C	O_A–C_A	Cu_A–N_A	Cu_A–N_B	Cu_B–N_C	Cu_B–N_D
3[a]	s	1.88	1.92	1.82	1.82	2.86	2.37	1.92	3.16	2.04	2.43	2.02	2.02
	s[b]	1.80	1.86	1.76	1.78	2.76	2.31	1.84	1.34	2.00	2.83	2.02	1.97
TS34	s	1.93	1.88	1.88	1.84	2.92	2.38	1.93	2.10	2.10	2.28	2.03	2.03
	t	1.96	1.95	1.88	1.85	2.90	2.48	2.08	2.26	2.08	2.30	2.07	2.07
4	so	2.07	1.90	2.01	1.89	2.88	2.66	2.12	1.43	2.18	2.22	2.07	2.12
	t	2.06	1.90	2.00	2.00	2.89	2.67	2.12	1.43	2.18	2.22	2.17	2.14

so open-shell singlet state, *s* closed-shell singlet state, *t* triplet state

[a] Only the singlet is reported, since the triplet for this structure lies much higher in energy

[b] Geometrical parameters corresponding to the structure equivalent to structure **3** found previously by Stack and coworkers [31]

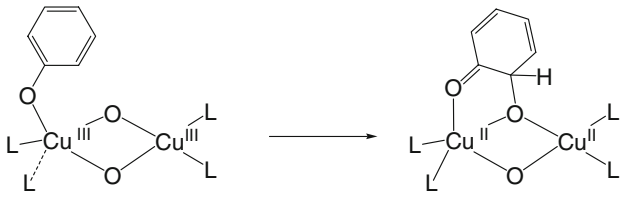

3 **4**

Scheme 8 C–O bond formation in the system studied

copper ions and an average distance of 1.92 Å of each copper with the four nitrogen/oxygen ligands (Table 5). Previously, Stack and coworkers [31] optimized a structure that corresponds to our structure **3** and the intermediate detected experimentally. It should be mentioned that their model includes the whole complex and the 2,4-di-*tert*-butylphenolate as a substrate, which is the substrate used experimentally. They used the unrestricted B3LYP hybrid functional with the 6-311G* basis set for the copper atoms and the 6-31G* basis set for each remaining atom. Despite using different models and basis sets, they obtained geometrical parameters that are quite similar to the ones that we found in the present study (Table 5).

In structure **3**, the attack on the ring by one of the oxygen atoms takes place (Scheme 8). The formation of a new C–O bond breaks the aromaticity of the phenolate and spin density appears on both copper ions (Table 6). Transition state TS34 was located for both the closed-shell singlet and the triplet cases. The singlet structure for TS34 (Fig. 3), with a barrier of 7.2 kcal/mol, is more stable than the triplet by 1 kcal/mol, but the structures are almost identical. In this step the distance between Cu_A–N_B decreases from 2.43 to 2.22 Å, while the distance between Cu_A–O_C increases from 1.92 to 2.12 Å. According to preliminary calculations at the B3LYP level by Stack and coworkers [31], the activation energy for the C–O bond formation step is 10.9 kcal/mol (a value of 12 kcal/mol is given in supporting information [31]). This value corresponds to the point of maximum energy along a linear transit that transforms **3** into **4** by approaching in successive steps the *ortho* carbon of the phenolate and the closest oxygen atom of the Cu_2O_2 core. No full optimization of the transition state was carried out in that work and, therefore, the barrier of 10.9 kcal/mol should be taken as an upper bound to the actual energy barrier [31]. Indeed, this value is higher by 3.7 kcal/mol than that obtained in the present work by fully optimizing the transition state structure. It is also worth noting that in a recent B3LYP study [70] using a similar basis set on a different $Cu_2O_2(L_2)^{2+}$ model, the authors were unable to locate a transition state similar to our TS34. Instead, they found a μ-η^1:η^1-Cu_2(I,II)O_2 intermediate that reacts to give a structure analogous of our structure **4** through a transition state with an energy barrier of about 16 kcal/mol. Despite several attempts to find it, such a μ-η^1:η^1-Cu_2(I,II)O_2 intermediate was not found on our potential energy surface.

Table 6 Spin density at different spin states for the structures that intervene in the C–O bond formation

Structures	Multiplicity	Spin density					ΔG
		Cu_A	Cu_B	O_A	O_B	Substrate	
3[a]	s[a]	–	–	–	–	–	−18.8
TS34	s	–	–	–	–	–	−11.6
	t	0.57	0.42	0.11	−0.10	0.80	−10.6
4	so	0.55	−0.47	0.00	−0.11	0.02	−44.9
	t	0.53	0.44	0.11	0.67	0.04	−46.2

Calculated free energies (G), relative to structure **1** plus the phenolate, in kilocalories per mole are also reported

so open-shell singlet state, *s* closed-shell singlet state, *t* triplet state

[a] Only the singlet is reported, since the triplet for this structures lies much higher in energy

The thermal decay rates at −105 °C for species **A** (see Scheme 6) formed with 6-*d*-2,4-di-*tert*-butylphenolate and

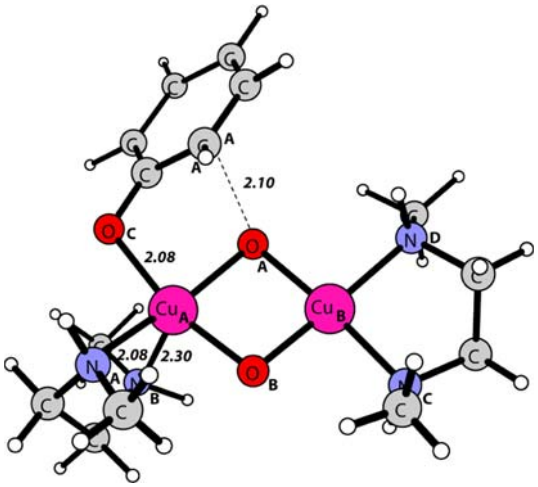

Fig. 3 Fully optimized transition state for the open-shell singlet state for C–O formation (TS34). Distances are in angstroms

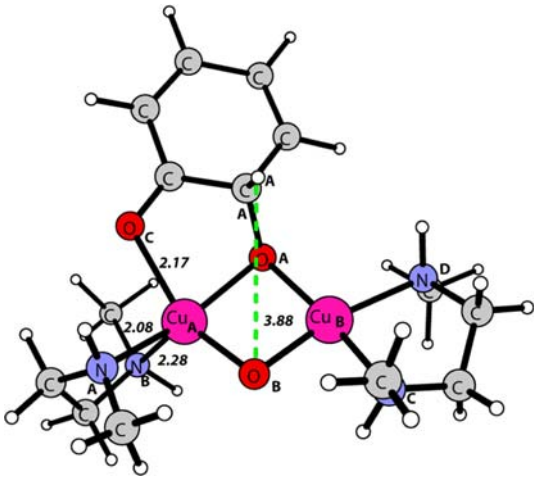

Fig. 4 Fully optimized transition state for the triplet state for rearrangement of the position of the substrate (TS45). Distances are in angstroms

6-*h*-2,4-di-*tert*-butylphenolate were measured by Stack and coworkers [31] and they obtained a kinetic isotope effect (KIE) of 0.83 ± 0.09. Using our model and the following expression derived from transition state theory [66]

$$\mathrm{KIE} = \frac{k_{\mathrm{H}}}{k_{\mathrm{D}}} = \frac{\frac{k_{\mathrm{B}}T}{h}(c^0)^{\Delta n}\mathrm{e}^{-\left(\Delta G_{\mathrm{H}}^{\neq}/RT\right)}}{\frac{k_{\mathrm{B}}T}{h}(c^0)^{\Delta n}\mathrm{e}^{-\left(\Delta G_{\mathrm{D}}^{\neq}/RT\right)}} = \mathrm{e}^{-\left(\left(\Delta G_{\mathrm{H}}^{\neq} - \Delta G_{D}^{\neq}\right)/RT\right)}, \quad (3)$$

we obtained a KIE of 0.88 at −105 °C, which is in excellent agreement with the reported experimental value. Such a small secondary inverse KIE is generally anticipated for electrophilic aromatic substitution reactions, in which a carbon center undergoes a hybridization change from sp^2 to sp^3 in the transition state. As it can be seen in Fig. 3, this is exactly what happens in TS34. The calculated free energy barrier of 7.2 kcal/mol and the KIE of 0.88 for the transformation of **3** into **4** perfectly matches the experimental 10.3 kcal/mol and 0.83 values, thus reinforcing the idea that this step is the rate-determining step for the transformation of **A** (Scheme 6) into the final products (but not for the full transformation from **0** to products!).

In structure **4** the distance between the hydrogen atom of the ring that has to be transferred and O_B is too long for the transfer to take place. For this reason there is a rearrangement of the position of the substrate that transforms **4** into **5** (Fig. 4 shows the transition state of this transformation). This reduces the O_B–H_A distance from 4.13 to 3.72 Å and increases the Cu_A–O_C distance from 2.12 to 2.40 Å. This step has a barrier of 0.3 kcal/mol with the small basis set. However, after the single-point-energy calculation is carried out with the bigger basis set and the effect of the solvent, the thermal corrections, and entropy effects are added, it turns out to be barrierless. It should be mentioned that for the experimentally reported $Cu_2O_2(DBED)_2^{2+}$ complex [31], owing to presence of the bulky *tert*-butyl substituents of the ligand, this step may possibly have a significant barrier since the whole system will have a larger steric hindrance for rotation.

After the rearrangement of the position of the substrate, the transfer of the hydrogen can finally occur (Scheme 9). The O_B–H_A distance goes from 3.72 Å in structure **5** to 0.97 Å in structure **6**. During this process, the ring of the substrate recovers the aromaticity (Table 7, Fig. 5). For this step, the open-shell singlet and triplet states both have a barrier of 4.7 kcal/mol (Table 7). As can be seen in Table 7, the geometrical parameters are almost identical for the two different spin states. Similar energies and geometries in the open-shell singlet and triplet states of **5** and also of TS56 are an indication that the two spins are weakly coupled for these species. Some spin density also appears on the ring after the hydrogen-atom transfer (Table 8, species **6**). The lack of spin density and the positive charge (0.47 *e*) on the hydrogen transferred in TS56 leads us to conclude that the process is a proton transfer in the transition state which is subsequently

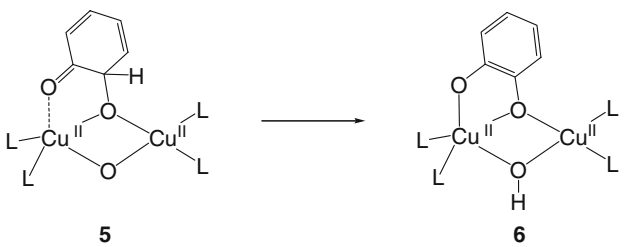

Scheme 9 Hydrogen-atom transfer in the system studied

Table 7 Comparison of geometrical parameters of the transition state for the structures that intervene in hydrogen-atom transfer

Structures	Multiplicity	Distances (Å)										
		Cu_A–O_A	Cu_A–O_B	Cu_B–O_A	Cu_B–O_B	Cu_A–Cu_B	O_A–O_B	O_A–C_A	Cu_A–N_A	Cu_A–N_B	C_A–H_A	O_B–H_A
5	so	2.09	1.89	2.03	1.87	2.89	2.66	1.43	2.09	2.14	1.12	3.72
	t	2.09	1.90	2.03	1.88	2.89	2.66	1.43	2.09	2.14	1.12	3.72
TS56	so	2.09	1.98	2.03	1.92	2.76	2.52	1.47	2.06	2.11	1.26	1.53
	t	2.09	1.98	2.04	1.93	2.76	2.51	1.47	2.06	2.11	1.26	1.52
6	so	2.03	2.02	2.04	1.94	3.00	2.61	1.38	2.06	2.23	4.77	0.97
	t	2.06	1.97	2.08	1.94	2.99	2.61	1.94	2.10	2.27	4.78	0.97

so open-shell singlet state, *t* triplet state

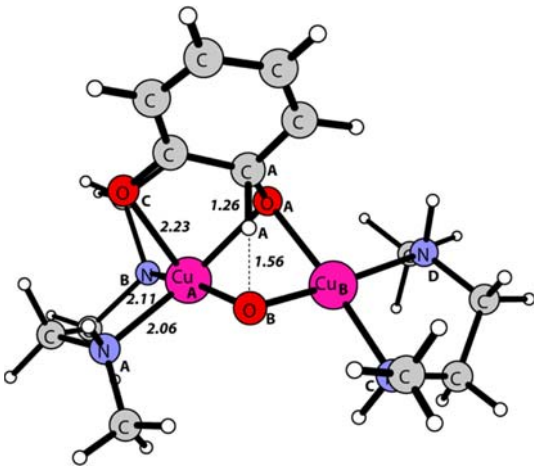

Fig. 5 Fully optimized transition state for the triplet state for the hydrogen-atom transfer (TS56). Distances are in angstroms

followed by an electron transfer. So, at the end, what has been transferred is a hydrogen atom, although in TS56 the particle transferred has to be considered a proton.

After the hydrogen-atom transfer, the last step of the reaction should consist of the transfer of two electrons from the complex, one from each of the copper ions, to the substrate to complete its reduction. This step is endothermic by 9.2 kcal/mol. This means that the barrier would probably be higher in energy than all the barriers found for the previous steps of the reaction that starts from structure **3**. However, it should be mentioned that experimentally an acid is added to obtain the products (the quinone and the catechol), so the added protons are probably necessary for the last stage of the reaction.

The free energies for the reaction mechanism studied in this work using the $Cu_2O_2(DMED)_2^{2+}$ complex are shown in Fig. 6. The reaction starts with the Cu_2-(II,II)-peroxo form of the complex in equilibrium with the Cu_2-(III,III)-bis-μ-oxo isomer and this is the situation when phenolate is added. At this stage, two scenarios are possible. Either the O–O bond cleavage takes place before the binding of the substrate, or the O–O bond cleaves after the binding of the substrate. Subsequently, the attack on the ring of one of the oxygen atoms occurs. To make possible the hydrogen-atom transfer from the ring to the second oxygen of the complex, a rearrangement of the position of the substrate takes place. Finally, the hydrogen atom is transferred from the substrate to the complex and the addition of protons would make possible the formation of the products, the quinone and the catechol, that are observed experimentally.

In both possible scenarios the most critical step is the peroxide O–O bond cleavage and this step is prior to the attack on the ring that leads to new C–O bond formation. For the step corresponding to the hydroxylation of the ring, the calculated free-energy barrier (7.2 kcal/mol) and KIE (0.88) are in good agreement with the experimental values (10.3 kcal/mol and 0.83, respectively), thus providing confidence about the validity of the results obtained.

Table 8 Spin density at different spin states for the structures that intervene in hydrogen-atom transfer

Calculated free energies (G), relative to structure **1** plus the phenolate, in kilocalories per mole are also reported

so open-shell singlet state, *t* triplet state

Structures	Multiplicity	Spin density					ΔG
		Cu_A	Cu_B	O_A	O_B	Substrate	
5	so	0.53	−0.47	−0.03	−0.03	0.01	−48.8
	t	0.50	0.44	0.15	0.65	0.01	−50.2
TS56	so	0.42	−0.53	0.04	0.08	0.01	−44.1
	t	0.50	0.40	0.30	0.52	0.00	−45.5
6	so	0.61	−0.41	−0.09	−0.02	−0.10	−93.7
	t	0.61	0.37	0.26	0.11	0.38	−94.3

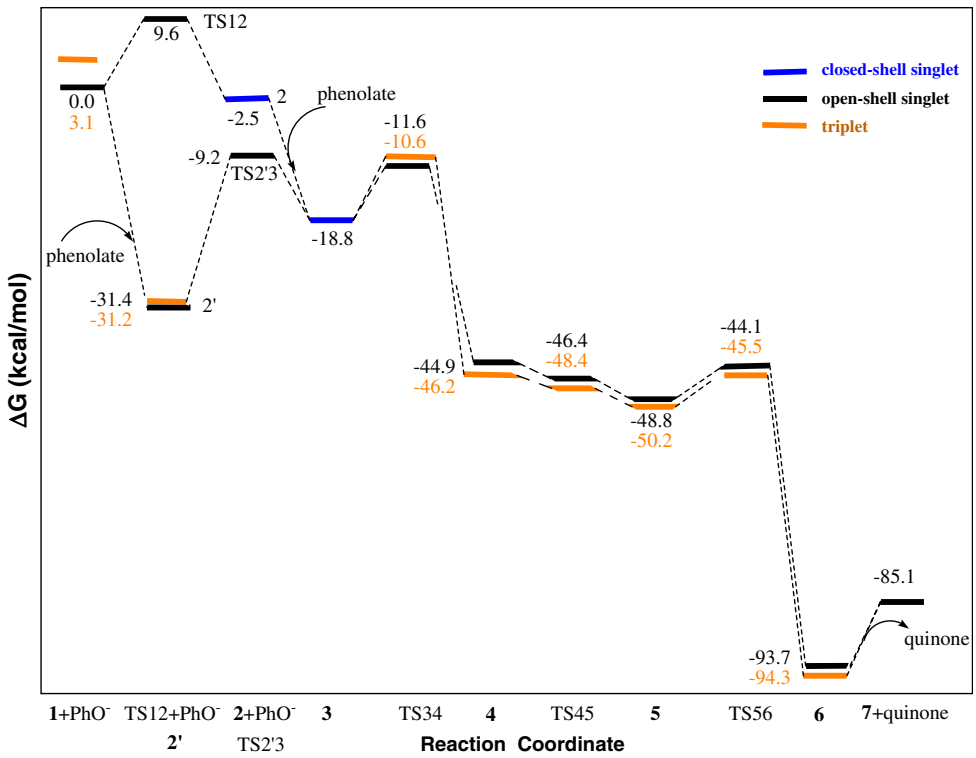

Fig. 6 Free-energy profile obtained for the mechanism studied at the B3LYP level of theory. Calculated free energies (G), relative to structure **1** plus phenolate, are given in kilocalories per mole

Table 9 Calculated free energies (G) in kilocalories per mole for different spin states for the structures that appear in the hydroxylation of phenolate for the model of the complex

Structures	B3LYP		B3LYP*	
	ΔG ($S = 0$)	ΔG ($S = 1$)	ΔG ($S = 0$)	ΔG ($S = 1$)
1 + PhO^-	0.0	1.9	0.0	4.0
TS12 + PhO^-	9.6	–	7.9	–
2 + PhO^-	−2.5	–	−7.2	–
2′	−31.4	−31.2	−30.8	−30.4
TS2′3	−9.2	–	−10.6	–
3	−18.8	–	−24.1	–
TS34	−11.6	−10.6	−17.4	−11.3
4	−44.9	−46.2	−43.3	−48.9
TS45	−46.4	−48.4	−44.7	−46.6
5	−48.8	−50.2	−47.2	−52.0
TS56	−44.1	−45.5	−44.0	−45.7
6	−93.7	−94.3	−92.8	−97.4
7	−85.1	–	−82.4	–

Finally, all the structures were also reoptimized using the B3LYP* functional, with only 15% HF exchange. As can be seen in Table 9, rather small effects were obtained from a decrease in the amount of exact exchange. The main changes occur for the relative energies of structures **2** and **3** with bis-μ-oxo character that, as discussed before (Table 2), are stabilized with the reduction of the HF exchange contribution to the hybrid density functional. For none of the intermediates or transition states, B3LYP and B3LYP* give different ground states. These results give further support to the reliability of the method used in the present work.

Before comparing the results obtained for the synthetic complex studied with the existing proposals for the catalytic cycle for tyrosinase, several facts have to be taken into account. For most of the biomimetic systems of tyrosinase, including the system studied in this article, the substrate is an anion, a phenolate, while for the enzyme the substrate is neutral, a phenol. Tyrosinase is thought to be capable of abstracting the proton of the phenol that it releases later to give the products. On the other hand, for the complex studied, protons have to be added in the last step of the reaction to obtain the quinone and/or the catechol. Moreover, since tyrosinase biomimetic complexes cannot restart the reaction by themselves, the reaction assisted by these compounds can be more exothermic than the reaction catalyzed by the enzyme.

In the proposal made by Solomon and coworkers [9, 71, 72] for the tyrosinase mechanism (Scheme 2), in the first step the phenol loses one proton before binding to one of the copper atoms of the active site. At his point, it should be highlighted that from the spectral features of oxytyrosinase Solomon and coworkers [71] proved that it has an active site very similar to that of oxyhemocyanin. For the tyrosinase mechanism, the O–O bond cleavage and the attack on the ring results in the formation of a coordinated o-diphenolate intermediate that has a simultaneous

coordination of the substrate to both copper centers in a bidentate bridging fashion [9, 72]. In our proposed mechanism for the hydroxylation of phenolates by $Cu_2O_2(DMED)_2^{2+}$ such a species does not intervene. The closest structure in our mechanism to the intermediate suggested by Solomon and coworkers for the enzyme catalytic cycle is species **6**, which has one of the oxygen atoms of the substrate bound to one of the copper ions and the other bound to both copper ions. For our model, we tried to locate a structure with the substrate coordinated to both copper centers in a bidentate bridging fashion as suggested by Solomon and coworkers [9]. Nevertheless, all attempts to find such species lead to structure **6** with only one of the oxygen atoms coordinated to both copper atoms. So, at least with the present model and level of calculation, the possibility of a reaction mechanism going through the intermediate suggested by Solomon and coworkers [9] has to be rejected in our model. Obviously, from our calculations the presence of such an intermediate cannot be ruled out in the reaction mechanism of tyrosinase.

In the mechanism suggested by Matoba et al. [11] (Scheme 4) for tyrosinase, the proton of the phenol does not leave the active site of the enzyme until the last step of the catalytic cycle. First, it is bound to one of the oxygen atoms of the peroxide moiety and then to His54. Later it forms the water molecule that is released in the last stage. Since for the present complex studied, the reaction starts with the phenolate and the protons are introduced to obtain products, comparisons cannot be made for this point. In the proposal of Matoba et al. [11], the binding mode of the substrate after the O–O bond cleavage and the attack on the ring is the same suggested by Solomon and coworkers. As said before, such intermediate was not found in the potential energy surface of our model.

It is also worth noting that in the proposals of both Solomon and coworkers and Matoba et al. the order in which the O–O bond cleavage and the attack on the ring occurs in the catalytic cycle for the phenolase activity of tyrosinase is not clearly specified and, therefore, it cannot be discussed in relation to our proposal. However, in both mechanisms, the O–O bond remains after the binding of the phenolate and the coordination environment of the two copper ions with the oxygen atoms, $Cu(II)_2$-μ-η^2:η^2-O_2, is not modified and this is at variance with the reaction mechanism reported in this work. In our theoretical study for the $Cu_2O_2(DMED)_2^{2+}$ complex, when the substrate is bound to one of the copper ions there are two possible coordination environments. A structure with an asymmetric $Cu(II)_2$-μ-η^1:η^2-O_2 core is proposed if the substrate binds to one of the copper ions prior to the O–O bond cleavage. On the other hand, a $Cu(III)_2$-(μ-O_2) structure is suggested after the O–O cleavage takes places, which corresponds to the intermediate observed experimentally by Stack and coworkers [31] (species **A** in Scheme 6).

Finally, our study for the $Cu_2O_2(DMED)_2^{2+}$ complex cannot be directly compared with the proposal made in the earlier hybrid DFT study by one of us for tyrosinase (Scheme 3) [10] for several reasons. In the first place, the total charge in the previous study was +1, while in the current model it is +2. Secondly, in that study the Cu_2-(II–II)-peroxo form of the complex that we use as the starting point for our mechanism does not appear. Finally, the previous mechanism involved an intermediate with a superoxo moiety that we have been unable to locate on our potential energy surface and not did not involve structure **3** (intermediate **A**) that has been detected experimentally.

Conclusions

In this work, we studied the full reaction mechanism of the hydroxylation of phenols mediated by the $Cu_2O_2(DMED)_2^{2+}$ complex. The proposed reaction mechanism follows an electrophilic aromatic substitution pattern that involves an intermediate with the O–O bond cleaved and the phenolate coordinated to a copper center. This species corresponds to the intermediate observed experimentally by Stack and coworkers [31]. The rate-determining step for the hydroxylation of this intermediate to the final products is the attack of one oxygen atom of the Cu_2O_2 unit on the aromatic ring leading to a new C–O bond. The barrier and the KIE for this ring hydroxylation step obtained with the B3LYP functional are in good agreement with the experimental results [31]. After this step, in our model complex, the reaction proceeds with smooth energy barriers until the final quinone products are reached. Unfortunately, our calculations cannot definitely assign whether the O–O cleavage takes place before or after the binding of the substrate. In our opinion, to get a definitive answer regarding these first steps of the reaction mechanism studied, it is necessary to include explicitly several solvent molecules in the model and to perform a study of the dynamics of the reaction. This is out of the scope of the present work but it will be the subject of future research in our laboratory.

Finally, although the results obtained refer only to the system studied, we consider that our study may offer some hints on the reaction mechanism of tyrosinase. For this reason, the existing proposals for the tyrosinase catalytic cycle mechanism and our theoretical mechanism for the $Cu_2O_2(DMED)_2^{2+}$ complex were compared and discussed as to the similarities and differences found.

Acknowledgments Financial help was furnished by the Spanish Ministerio de Educación y Ciencia (MEC) projects no. CTQ2005-08797-C02-01/BQU and CTQ2008-03077/BQU and by the Catalan

Departament d'Universitats, Recerca i Societat de la Informació (DURSI) of the Generalitat de Catalunya project no. 2005SGR-00238. We thank Miquel Costas for valuable discussions and the reviewers for helpful comments. M.G. thanks the Spanish MEC for a Ph.D. grant.

References

1. Solomon EI, Sundaram UM, Machonkin TE (1996) Chem Rev 96:2563–2605
2. Solomon EI, Baldwin MJ, Lowery MD (1992) Chem Rev 92:521–542
3. Oetting WS (2000) Pigment Cell Res 13:320–325
4. Xu YM, Stokes AH, Roskoski R, Vrana KE (1998) J Neurosci Res 54:691–697
5. Asanuma M, Miyazaki I, Ogawa N (2003) Neurotox Res 5:165–176
6. Parvez S, Kang M, Chung HS, Bae H (2007) Phytother Res 21:805–816
7. de Faria RO, Moure VR, Amazonas M, Krieger N, Mitchell DA (2007) Food Technol Biotechnol 45:287–294
8. Sánchez-Ferrer A, Rodríguez-López JN, García-Cánovas F, García-Carmona F (1995) Biochim Biophys Acta Protein Struct Mol Enzymol 1247:1–11
9. Wilcox DE, Porras AG, Hwang YT, Lerch K, Winkler ME, Solomon EI (1985) J Am Chem Soc 107:4015–4027
10. Siegbahn PEM (2003) J Biol Inorg Chem 8:567–576
11. Matoba Y, Kumagai T, Yamamoto A, Yoshitsu H, Sugiyama M (2006) J Biol Chem 281:8981–8990
12. Ross PK, Solomon EI (1990) J Am Chem Soc 112:5871–5872
13. Ross PK, Solomon EI (1991) J Am Chem Soc 113:3246–3259
14. Baldwin MJ, Root DE, Pate JE, Fujisawa K, Kitajima N, Solomon EI (1992) J Am Chem Soc 114:10421–10431
15. Eickman NC, Solomon EI, Larrabee JA, Spiro TG, Lerch K (1978) J Am Chem Soc 100:6529–6531
16. Lewis EA, Tolman WB (2004) Chem Rev 104:1047–1076
17. Hatcher LQ, Karlin KD (2004) J Biol Inorg Chem 9:669–683
18. Hatcher LQ, Karlin KD (2006) Adv Inorg Chem Bioinorg Stud 58:131–184
19. Costas M, Ribas X, Poater A, López Balvuena JM, Xifra R, Company A, Duran M, Solà M, Llobet A, Corbella M, Usón MA, Mahía J, Solans X, Shan X, Benet-Buchholz J (2006) Inorg Chem 45:3569–3581
20. Ribas X, Xifra R, Parella T, Poater A, Solà M, Llobet A (2006) Angew Chem Int Ed 45:2941–2944
21. Brackman W, Havinga E (1955) Recl Trav Chim Pays Bas 74:1021–1039
22. Brackman W, Havinga E (1955) Recl Trav Chim Pays Bas 74:1070–1080
23. Brackman W, Havinga E (1955) Recl Trav Chim Pays Bas 74:1100–1106
24. Brackman W, Havinga E (1955) Recl Trav Chim Pays Bas 74:1107–1118
25. Brackman W, Havinga E (1955) Recl Trav Chim Pays Bas 74:937–955
26. Karlin KD, Cruse RW, Gultneh Y, Hayes JC, Zubieta J (1984) J Am Chem Soc 106:3372–3374
27. Nasir MS, Cohen BI, Karlin KD (1992) J Am Chem Soc 114:2482–2494
28. Karlin KD, Nasir MS, Cohen BI, Cruse RW, Kaderli S, Zuberbuhler AD (1994) J Am Chem Soc 116:1324–1336
29. Pidcock E, Obias HV, Zhang CX, Karlin KD, Solomon EI (1998) J Am Chem Soc 120:7841–7847
30. Palavicini S, Granata A, Monzani E, Casella L (2005) J Am Chem Soc 127:18031–18036
31. Mirica LM, Vance M, Rudd DJ, Hedman B, Hodgson KO, Solomon EI, Stack TDP (2005) Science 308:1890–1892
32. Mirica LM, Ottenwaelder X, Stack TDP (2004) Chem Rev 104:1013–1045
33. Que L, Tolman WB (2002) Angew Chem Int Ed 41:1114–1137
34. Becke AD (1993) J Chem Phys 98:5648–5652
35. Lee CT, Yang WT, Parr RG (1988) Phys Rev B 37:785–789
36. Schrödinger (2003) Jaguar 5.5. Schrödinger, Portland
37. Hay PJ, Wadt WR (1985) J Chem Phys 82:299–310
38. Frisch MJ, Trucks GW, Schlegel HB, Scuseria GE, Robb MA, Cheeseman JR, Montgomery JA Jr, Vreven T, Kudin KN, Burant JC, Millam JM, Iyengar SS, Tomasi J, Barone V, Mennucci B, Cossi M, Scalmani G, Rega N, Petersson GA, Nakatsuji H, Hada M, Ehara M, Toyota K, Fukuda R, Hasegawa J, Ishida M, Nakajima T, Honda Y, Kitao O, Nakai H, Klene M, Li X, Knox JE, Hratchian HP, Cross JB, Bakken V, Adamo C, Jaramillo J, Gomperts R, Stratmann RE, Yazyev O, Austin AJ, Cammi R, Pomelli C, Ochterski JW, Ayala PY, Morokuma K, Voth GA, Salvador P, Dannenberg JJ, Zakrzewski G, Dapprich S, Daniels AD, Strain MC, Farkas O, Malick DK, Rabuck AD, Raghavachari K, Foresman JB, Ortiz JV, Cui Q, Baboul AG, Clifford S, Cioslowski J, Stefanov BB, Liu G, Liashenko A, Piskorz P, Komaromi I, Martin RL, Fox DJ, Keith T, Al-Laham MA, Peng CY, Nanayakkara A, Challacombe M, Gill PMW, Johnson B, Chen W, Wong MW, Gonzalez C, Pople JA (2003) Gaussian 03. Gaussian, Pittsburgh
39. Dunning TH (1989) J Chem Phys 90:1007–1023
40. Woon DE, Dunning TH (1994) J Chem Phys 100:2975–2988
41. Tannor DJ, Marten B, Murphy R, Friesner RA, Sitkoff D, Nicholls A, Ringnalda M, Goddard WA, Honig B (1994) J Am Chem Soc 116:11875–11882
42. Marten B, Kim K, Cortis C, Friesner RA, Murphy RB, Ringnalda MN, Sitkoff D, Honig B (1996) J Phys Chem 100:11775–11788
43. Curtiss LA, Raghavachari K, Redfern PC, Pople JA (2000) J Chem Phys 112:7374–7383
44. Siegbahn PEM, Blomberg MRA (1999) Annu Rev Phys Chem 50:221–249
45. Salomon O, Reiher M, Hess BA (2002) J Chem Phys 117:4729–4737
46. Reiher M, Salomon O, Hess BA (2001) Theor Chem Acc 107:48–55
47. Cramer CJ, Tolman WB (2007) Acc Chem Res 40:601–608
48. Lewin JL, Heppner DE, Cramer CJ (2007) J Biol Inorg Chem 12:1221–1234
49. Cramer CJ, Kinal A, Wloch M, Piecuch P, Gagliardi L (2006) J Phys Chem A 110:11557–11568
50. Cramer CJ, Kinal A, Wloch M, Piecuch P, Gagliardi L (2007) J Phys Chem A 111:4871
51. Siegbahn PEM (2003) J Biol Inorg Chem 8:577–585
52. Cramer CJ, Wloch M, Piecuch P, Puzzarini C, Gagliardi L (2006) J Phys Chem A 110:1991–2004
53. Malmqvist PA, Pierloot K, Shahi ARM, Cramer CJ, Gagliardi L (2008) J Chem Phys 128:204109–204110
54. Gherman B, Cramer C (2008) Coord Chem Rev. doi: 10.1016/j.ccr.2007.11.018
55. Mirica L (2005) PhD thesis, Standford University. Available via the ProQuest database, UMI # 3162369
56. Mirica LM, Rudd DJ, Vance MA, Solomon EI, Hodgson KO, Hedman B, Stack TDP (2006) J Am Chem Soc 128:2654–2665
57. Becke AD (1988) Phys Rev A 38:3098–3100
58. Perdew JP, Chevary JA, Vosko SH, Jackson KA, Pederson MR, Singh DJ, Fiolhais C (1992) Phys Rev B 46:6671–6687
59. Perdew JP, Burke K, Wang Y (1996) Phys Rev B 54:16533–16539

60. Stephens PJ, Devlin FJ, Chabalowski CF, Frisch MJ (1994) J Phys Chem 98:11623–11627
61. Vosko SH, Wilk L, Nusair M (1980) Can J Phys 58:1200–1211
62. Hertwig RH, Koch W (1997) Chem Phys Lett 268:345–351
63. Gherman BF, Tolman WB, Cramer CJ (2006) J Comput Chem 27:1950–1961
64. Burke K, Ernzerhof M, Perdew JP (1997) Chem Phys Lett 265:115–120
65. Becke AD (1996) J Chem Phys 104:1040–1046
66. Atkins P, De Paula J (2006) Physical chemistry. Oxford University Press, Oxford
67. Mahadevan V, Henson MJ, Solomon EI, Stack TDP (2000) J Am Chem Soc 122:10249–10250
68. Hatcher LQ, Vance MA, Sarjeant AAN, Solomon EI, Karlin KD (2006) Inorg Chem 45:3004–3013
69. Itoh S, Taki M, Nakao H, Holland PL, Tolman WB, Que L, Fukuzumi S (2000) Angew Chem Int Ed 39:398–400
70. Naka H, Kondo Y, Usui S, Hashimoto Y, Uchiyama M (2007) Adv Synth Catal 349:595–600
71. Himmelwright RS, Eickman NC, Lubien CD, Lerch K, Solomon EI (1980) J Am Chem Soc 102:7339–7344
72. Winkler ME, Lerch K, Solomon EI (1981) J Am Chem Soc 103:7001–7003